LARGE EDDY SIMULATIONS OF SMOKE MOVEMENT

by

**K.B. McGrattan, H.R. Baum and
R.G. Rehm
Building and Fire Research Laboratory
National Institute of Standards and Technology
Gaithersburg, MD 20899   USA**

Large Eddy Simulations of Smoke Movement

K. B. McGrattan,* H. R. Baum & R. G. Rehm

National Institute of Standards and Technology, Gaithersburg, Maryland, USA

ABSTRACT

An approach to field modeling of fire phenomena in enclosures is presented. The conservation equations of mass, momentum and energy are calculated with sufficient temporal and spatial resolution to yield a truly three-dimensional, dynamic picture of the fire plume and its surroundings. The large-scale eddies are simulated directly and sub-grid scale motion is represented by a constant eddy viscosity. Efficient flow solving techniques make it possible to simulate fire scenarios using computational grids in excess of a million cells on modern workstations. Several examples of the methodology are presented. © *1998 Published by Elsevier Science Ltd. All rights reserved.*

1 INTRODUCTION

In the past decade, field modeling of fire-related phenomena has increased dramatically due in large part to the availability of powerful, reasonably priced computers and the development of general purpose, easy to use software packages. While this has been met with enthusiasm from the fire research community, there is still considerable debate as to the direction of future research in this area. A great emphasis has been placed on the development of sophisticated grid generation algorithms and complex sub-models describing radiation, species generation, flame spread, and so on. No doubt these are important issues to consider, but the increased complexity of the models due to the inclusion of all these features in most instances limits the spatial resolution of the computational grid. Some insist that the use of turbulence models compensates for the loss of resolution,[1] but as the variety of applications increases, it is unclear what the effects of the various turbulence parameters are on the solution, and indeed, what the solution actually represents.

---

*Author to whom correspondence should be addressed. Tel.: 301 975 2712; Fax: 301 975 9647.

Our approach to field modeling fire phenomena emphasizes high spatial resolution and efficient flow solving techniques. The large-scale eddies that govern the mixing of the gases are directly simulated on as fine a scale as the underlying computational grid will allow. Sub-grid scale motion is idealized by a constant eddy viscosity. This technique is a very simple type of 'large eddy simulation', a phrase describing a class of turbulence models that were originally developed by Smagorinsky[2] to study large-scale circulation in the atmosphere. The idea is to distinguish large-scale motions that can be explicitly resolved in the computation from those that are 'sub-grid' scale. These latter motions are represented by an eddy viscosity whose length scale is tied to the grid used in the calculations, and whose time scale is determined by the local resolvable dissipation. This pioneering work led to a large literature in the turbulence modeling community whose object is the development of improvements to Smagorinsky's treatment. It is worth noting, however, that few if any of these models have been adopted by the meteorology community. In fact, the systematic improvements in predictive capacity that have taken place over the past 25 years have been due to two lines of research: the development of sophisticated models of other atmospheric phenomena that are irrelevant in the present context, and systematic improvements in spatial and temporal resolution that are crucial to understanding the approach taken in this paper. The critical issue, both in the prediction of atmospheric circulation and fire-induced convection, is the ability to calculate the flow at high enough spatial and temporal resolution. The criteria that must be satisfied are, of course, very different for the two fields. A useful guide for fire-induced flows is set out below. The range of length scales that must be left unresolved is much smaller in any fire scenario than in meteorology. We have taken advantage of this by simplifying the approach further and replacing the viscosity by a constant. Thus, we are left with the Navier–Stokes equations as the mathematical model on which the computations are based.

This approach has been fostered by the ever-increasing power of computers and the development of faster numerical algorithms. To make the most of the current generation workstations, we have focused our efforts on developing relatively simple numerical algorithms to address the transport of combustion products in single or multi-room enclosures, gridded uniformly in the horizontal directions, with the option of variable gridding in the vertical direction. Great efficiency is obtained by embedding the enclosures within either rectangular or cylindrical domains, creating walls and doorways by masking off grid cells. Because simulations involving over a million grid cells are not difficult, fairly elaborate geometries can be considered without sacrificing spatial resolution.

The transport of combustion products is calculated directly from an approximate form of the Navier–Stokes equations. This approximation involves

the filtering out of acoustic waves while allowing for large variations in temperature and density.[3] Some refer to these equations as 'weakly compressible' or 'thermally expandable'. The terms emphasize the elliptic character of the equations, consistent with low speed, thermal convective processes. The fire itself is prescribed in a manner consistent with a mixture fraction-based approach to combustion, but the combustion phenomena themselves are not simulated. Lagrangian particles representing burning fuel are introduced into the flow domain and collectively represent the fire. The section describing these 'thermal elements' provides a mathematical justification for this procedure based on the low Mach number equations for diffusion-controlled combustion. The level of complexity involved in prescribing the burning history of the fuel elements depends on the scenario of interest and the available spatial resolution.

2 HYDRODYNAMIC MODEL

We consider a thermally expandable ideal gas driven by a prescribed heat source. The motion of the fluid is governed by the equations written in a form suitable for low Mach number applications:[3]

$$\frac{\partial \rho}{\partial t} + \nabla \cdot \rho \mathbf{u} = 0 \tag{1}$$

$$\rho \left(\frac{\partial \mathbf{u}}{\partial t} + \frac{1}{2} \nabla |\mathbf{u}|^2 - \mathbf{u} \times \omega \right) + \nabla p - \rho \mathbf{g} = \nabla \cdot \sigma \tag{2}$$

$$\rho c_p \left(\frac{\partial T}{\partial t} + \mathbf{u} \cdot \nabla T \right) - \frac{dp_0}{dt} = \dot{q} + \nabla \cdot k \nabla T \tag{3}$$

$$p_0(t) = \rho \mathscr{R} T \tag{4}$$

Here, all symbols have their usual fluid dynamical meaning: ρ is the density, $\mathbf{u}$ the velocity vector, ω the vorticity, p the pressure, $\mathbf{g}$ the gravity vector, c_p the constant pressure specific heat, T the temperature, k the thermal conductivity, t the time, $\dot{q}$ the prescribed volumetric heat release, $\mathscr{R}$ the gas constant equal to the difference of the specific heats $\mathscr{R} = c_p - c_v$, and σ the standard stress tensor for compressible fluids. Notice in the energy and state equations that the spatially and temporally varying pressure has been replaced by an average pressure p_0 that depends only on time. This approximation is made to filter out acoustic waves, and it is the reason that the equations are referred to as weakly compressible.

The divergence of the flow $\nabla \cdot \mathbf{u}$ is a very important quantity in the analysis to follow, and it is readily found by combining eqns (1) and (3) and using the

equation of state, eqn (4),

$$p_0 \nabla \cdot \mathbf{u} + \frac{1}{\gamma} \frac{\mathrm{d}p_0}{\mathrm{d}t} = \frac{\gamma - 1}{\gamma} (\dot{q} + \nabla \cdot k \nabla T) \tag{5}$$

where $\gamma = c_p/c_v$. Integrating eqn (5) over the entire domain Ω yields a consistency condition for the background pressure $p_0(t)$

$$\frac{V}{\gamma} \frac{\mathrm{d}p_0}{\mathrm{d}t} = \frac{\gamma - 1}{\gamma} \left(\int_\Omega \dot{q} \mathrm{d}V + \int_{\partial\Omega} k \nabla T \, \mathrm{d}\mathbf{S} \right) - p_0 \int_{\partial\Omega} \mathbf{u} \cdot \mathrm{d}\mathbf{S} \tag{6}$$

where V is the volume of the enclosure. Equation (6) shows that the background pressure is increased by the addition of heat, and decreased by the net volume outflow together with conductive heat losses at the boundaries.

The background pressure can be expressed in terms of a background temperature $T_0(t)$ and density $\rho_0(t)$

$$p_0 = \mathscr{R} \rho_0 T_0 \tag{7}$$

These spatially averaged quantities play the same role that ambient conditions do in the Boussinesq approximation. Perturbations to each are represented by the relations

$$T = T_0(t)(1 + \tilde{T}), \qquad \rho = \rho_0(t)(1 + \tilde{\rho}) \tag{8}$$

and p_0 and ρ_0 are related through the adiabatic process

$$\frac{\rho_0}{\rho_\infty} = \left(\frac{p_0}{p_\infty} \right)^{1/\gamma} \tag{9}$$

Using these relationships allows the energy equation to be expressed in terms of the perturbation temperature $\tilde{T}$ and the divergence

$$\frac{\partial \tilde{T}}{\partial t} + \mathbf{u} \cdot \nabla \tilde{T} = (1 + \tilde{T}) \left[\nabla \cdot \mathbf{u} + \frac{1}{\gamma p_0} \frac{\mathrm{d}p_0}{\mathrm{d}t} \right] \tag{10}$$

The background pressure is found from eqn (6). Usually the background quantities remain at their ambient values unless the enclosure is tightly sealed.

Next, we simplify the momentum equation. The pressure is composed of three components, the background $p_0(t)$, the hydrostatic, and a perturbation to the hydrostatic $\tilde{p}$

$$p(\mathbf{r}, t) = p_0(t) - \rho_0(t)gz + \tilde{p}(\mathbf{r}, t) \tag{11}$$

where z is the vertical spatial component. We subtract off the hydrostatic pressure gradient from the momentum eqn (2), and then divide by the density

to obtain

$$\frac{\partial \mathbf{u}}{\partial t} + \frac{1}{2} V |\mathbf{u}|^2 - \mathbf{u} \times \omega + \frac{1}{\rho} V \tilde{p} - \frac{\rho - \rho_0}{\rho} \mathbf{g} = \frac{1}{\rho} V \cdot \sigma \qquad (12)$$

To simplify this equation further, the density in the pressure term is assumed ambient, and then the term $|\mathbf{u}|^2/2$ is combined with the perturbation pressure $\tilde{p}/\rho_0$ and written as a total pressure, $\mathcal{H}$. The replacement of the local density by its ambient value in the pressure gradient term implies that the vorticity generation induced by buoyancy is much more important than that due to baroclinic effects (i.e. the non-alignment of the pressure and density gradients). This is simply a computationally convenient way of defining a buoyancy-driven flow. While the assumption breaks down at scales small enough for molecular diffusion to be an important process (as in individual flame sheets), it is an excellent approximation of the computationally resolvable length scales. Finally, if the coefficient of viscosity is assumed constant, the momentum equation can be written

$$\frac{\partial \mathbf{u}}{\partial t} - \mathbf{u} \times \omega + V\mathcal{H} + \tilde{T}\mathbf{g} = v(\tfrac{4}{3}V(V \cdot \mathbf{u}) - V \times \omega) \qquad (13)$$

For most applications, the effective kinematic viscosity coefficient v represents dissipation on length scales below the resolution limits of the calculation. The effective Reynolds number is high enough to permit direct simulation of convective motion over a spatial range of two orders of magnitude for a three-dimensional calculation.

3 THERMAL ELEMENTS

The fire is represented by introducing a large number of Lagrangian elements that release heat as they are convected about by the thermally induced motion. Since the fluid motion determines where the heat is actually released, and the heat release determines the motion, the large-scale features of the coupling between the fire and the smoke transport are retained. It should be noted, however, that the heat release rate is *not* predicted, but is an input parameter in the computer programs implementing this model. The smoke is simulated by tracking the convected elements after the fuel burnout is completed. A specified percentage of the fuel consumed is assumed to be converted to smoke particulate. Thus, a knowledge of the spatial distribution of the Lagrangian elements is equivalent to a specification of the smoke particulate density at any instant of time.

The theoretical basis for the thermal element combustion model can be readily deduced from the mixture fraction representation of an isolated fire

plume. Denoting this quantity by $Z(\mathbf{r}, t)$, it is a solution to the equation:

$$\rho\left(\frac{\partial}{\partial t} + \mathbf{u} \cdot \boldsymbol{\nabla}\right)Z = \boldsymbol{\nabla} \cdot (\rho D \boldsymbol{\nabla} Z) \qquad (14)$$

The velocity vector $\mathbf{u}$ can always be decomposed into a solenoidal component $\mathbf{v}$ and an irrotational component $\boldsymbol{\nabla}\phi$. The solenoidal component is by definition divergence free, while the potential flow carries the expansion of the gas induced by the combustion heat release. This follows from the mass conservation equation that can be written in the form:

$$\left(\frac{\partial}{\partial t} + \mathbf{u} \cdot \boldsymbol{\nabla}\right)\rho + \rho \boldsymbol{\nabla} \cdot \mathbf{u} = 0 \qquad (15)$$

Since by hypothesis $\rho = \rho(Z)$, combining eqns (14) and (15) with the velocity decomposition described above yields the following equation for the potential function:

$$\boldsymbol{\nabla}^2 \phi = \frac{d(1/\rho)}{dZ} \boldsymbol{\nabla} \cdot (\rho D \boldsymbol{\nabla} Z) \qquad (16)$$

Equation (16) clearly relates the potential flow to the mixture fraction and hence the combustion heat release. The next step is the assumption that the gasified fuel emerging from the condensed phase is rapidly broken up into isolated deforming blobs of reacting fuel surrounded by air. The mechanism controlling the break-up process is the local strain field generated by the fire. Under this assumption, the fire is a large collection of objects described and visualized by Baum et al.[4] In this view, each blob is carried along by the large-scale motion and deformed by the local mixing that controls the combustion process in the blob.

The potential associated with each fuel blob can be expressed in terms of a modified mixture fraction $F(Z)$

$$F(Z) = \frac{\int_0^Z \rho(Z)D(Z)\,dZ}{\int_0^1 \rho D\,dZ} \qquad (17)$$

The specific volume $1/\rho$ is assumed to be a piecewise linear function of the mixture fraction on each side of the flame. Then two fuel-dependent constants K_+ and K_- can be defined, one for each side of the flame. They are

$$K_+ = \frac{d(1/\rho)}{dZ} \int_0^1 \rho D\,dZ, \quad (Z < Z_{fl}) \qquad (18)$$

$$K_- = \left|\frac{d(1/\rho)}{dZ}\right| \int_0^1 \rho D\,dZ, \quad (Z > Z_{fl}) \qquad (19)$$

Here, Z_{fl} denotes the value of the mixture fraction at the flame sheet associated with the individual bob. Note that fuel exists only where $Z > Z_{fl}$ and oxidant only where $Z < Z_{fl}$. The solution for ϕ can now be written as

$$\phi = - K_-F(Z) + \phi_H, \quad (Z > Z_{fl})$$

$$\phi = + K_+F(Z) + \phi_H, \quad (Z < Z_{fl}) \tag{20}$$

$$\phi_H = \frac{1}{4\pi} \oint dS_{fl} \nabla F \cdot \mathbf{n}_{fl} \frac{(K_+ + K_-)}{|\mathbf{r} - \mathbf{r}_{fl}|} \tag{21}$$

The integral in eqn (21) is taken over the flame surface, with $\mathbf{n}_{fl}$ denoting the outward pointing normal to the surface and $\mathbf{r}_{fl}$ a point on the flame.

The solution expressed by eqns (20) and (21) can be interpreted as follows. Each fuel containing element is convected in a large-scale flow field described by

$$\mathbf{u} = \mathbf{v} + \sum_n \nabla \phi_H(\mathbf{r} - \mathbf{r}_n, t) \tag{22}$$

Here, the sum is over the far-field approximation to the expansion field induced by all the blobs, while $\mathbf{v}$ denotes the composite solenoidal velocity field. Writing $\phi_H(\mathbf{r} - \mathbf{r}_n, t)$ out explicitly:

$$\phi_H(\mathbf{r} - \mathbf{r}_n, t) = \frac{1}{4\pi|\mathbf{r} - \mathbf{r}_n|} \oint dS_{fl} \nabla F \cdot \mathbf{n}_{fl} (K_+ + K_-) \tag{23}$$

The quantity $\mathbf{r}_n$ is the centroid of the instantaneous surface of the flame sheet. Note that this is the solution corresponding to a point source of volume generated by the combustion heat release.

The precise location of $\mathbf{r}_n$ is irrelevant at scales much larger than the fuel blob. The important quantity in eqn (23) is the integral that is proportional to the heat release associated with the blob. The direct calculation of this quantity would require the solution of the equations of motion including the mixture fraction down to length scales small enough to capture the local mixing and diffusion on the scale of the fuel element. This is not feasible at present, since the active combustion zone of a fire is usually only a small fraction of the space that must be included in any simulation. This leaves two choices; either extract the equivalent information from a local model of the combustion processes at the scale of the fuel element (see Baum *et al.*[4] for a preliminary calculation along these lines) or obtain the information empirically. In the present paper, the latter procedure is followed. The heat release rate $\dot{q}_n(t)$ associated with the nth element is represented by a simple function with a time scale determined from the plume correlations summarized by Baum and McCaffrey.[5] The heat released from each individual particle is

interpolated onto the computational grid, and the particles are advected by the resulting flow field.

The heat release rate from each thermal element is reduced by a prescribed fraction to account for radiative losses from the fire. At present, this radiation is lost to the system. Clearly, in an enclosure fire it will make a contribution to heating the enclosure boundaries. For problems in which this 'conjugate heat transfer' is of interest, the effect on the fluid motion can be important. At the present stage of model development, the wall temperature is either fixed at ambient values (short-time simulations) or the wall is assumed to be adiabatic (quasi-steady conditions). There is nothing inherent in the present approach requiring either assumption, and it is anticipated that these restrictions will be removed in the future.

4 NUMERICAL METHOD

The equations that are solved numerically are the energy eqn (10), the momentum eqn (13), and a Poisson equation for the total pressure, obtained by taking the divergence of eqn (13). The background pressure, temperature and density are found from eqns (6), (7) and (9). Each of the conservation equations emphasize the importance of the divergence and vorticity fields, as well as the close relationship between the thermally expandable fluid equations[3] and the Boussinesq equations for which the authors have developed highly efficient solution procedures.[6,7] All spatial derivatives are approximated by second-order central differences and the flow variables are updated in time using an explicit second-order Runge–Kutta scheme. The grid is taken to be uniform in the horizontal directions, but is allowed to vary arbitrarily in the vertical direction. Within each computational cell, vector components are evaluated at the sides, scalar quantities at the center.

The equation for the total pressure $\mathscr{H}$ is an elliptic partial differential equation of the form

$$\nabla^2 \mathscr{H} = -\frac{\partial \nabla \cdot \mathbf{u}}{\partial t} - \nabla \cdot \mathbf{F} \tag{24}$$

where the vector $\mathbf{F}$ represents the convective and diffusive terms of the momentum equation. The linear algebraic system arising from the discretization of eqn (24) has constant coefficients and can be solved to machine accuracy by a fast, direct (i.e. non-iterative) method that utilizes fast Fourier transforms. No-flux boundary conditions are specified by asserting that

$$\frac{\partial \mathscr{H}}{\partial n} = -F_n \tag{25}$$

at solid walls, where F_n is the normal component of **F** at the wall. This equation asserts that the normal component of velocity at the wall does not change with time, and indeed remains zero assuming the flow velocity is initially zero. At open external boundaries it is assumed that the perturbation pressure is known, but there are numerous other strategies for prescribing open boundary conditions that will not be discussed here.[8]

Direct Poisson solvers are most efficient if the domain is a rectangular region, although other geometries such as cylinders and spheres can be handled almost as easily. For these solvers, the no-flux condition of eqn (25) is simple to prescribe at external boundaries. However, many practical problems involve more complicated geometries. For building fires, doors and windows within multi-room enclosures are very important features of the simulations. These elements may be included in the overall domain as masked grid cells, but the no-flux condition of eqn (25) cannot be directly prescribed at the boundaries of these blocked cells due to consistency issues. However, it is possible to exploit the relatively small changes in the pressure from one time step to the next to enforce the no-flux condition. At the start of a time step, the components of the convection/diffusion term **F** are computed at all cell faces that do not correspond to walls. Then, at those cell faces that do, set

$$F_n = -\frac{\partial \mathcal{H}^*}{\partial n} + \beta u_n \tag{26}$$

where F_n is the normal component of **F** at the wall, and β is a relaxation factor empirically determined to be about 0·8 divided by the time step. The asterisk indicates the most recent value of the pressure. This modification only affects the right-hand side of eqn (24); thus the Poisson solver does not have to be modified to accommodate the internal blockages. Equation (26) asserts that following the solution of the Poisson equation for the pressure, the normal component of velocity u_n will be driven closer to zero according to

$$\frac{\partial u_n}{\partial t} \approx -\beta u_n \tag{27}$$

This is approximate because the true value of the velocity time derivative depends on the solution of the pressure equation, but since the most recent estimate of pressure is used, the approximation is very good. Also, even though there are small errors in normal velocity at solid surfaces, the divergence of each blocked cell remains exactly zero for the duration of the calculation, and the consistency condition of eqn (6) ensures global mass conservation. In other words, the total flux into a given obstacle is always identically zero, and the error in normal velocity is usually at least 3 or 4 orders of magnitude smaller than the characteristic flow velocity. When

implemented as part of a predictor–corrector updating scheme, the no-flux condition at solid surfaces is maintained remarkably well.

The speed and accuracy of this technique enable calculations on current generation workstations which involve over a million computational cells, yielding the spatial dynamic range of two orders of magnitude for a three-dimensional calculation. Presently, these computations require approximately 12 μs per cell per time step on an IBM RS 6000/58H server, and use several hundred megabytes of memory. The large memory requirement is not a problem, since memory is now relatively inexpensive. With this speed, computations involving over a million grid cells can be done in about 24 h. Simulations with only tens of thousands of grid cells (usually the limit of most commercial packages) can be done in less than 1 h.

5 RESULTS

Before presenting specific results, it is important to understand what length scales must be resolved in order to have a true predictive capability. For a fire plume, the characteristic length scale is related to the total heat release rate $\dot{Q}$ by the relation[5]

$$D^* = \left(\frac{\dot{Q}}{\rho_\infty T_\infty c_\mathrm{p} \sqrt{g}} \right)^{2/5} \tag{28}$$

Careful comparisons with plume correlations indicate that adequate resolution is achieved when this characteristic length D^* is spanned by roughly ten computational cells. Indeed, if the equations of motion are normalized using D^* as the length scale and $\sqrt{g D^*}$ as the velocity scale, the resulting equations would contain only a Reynolds number as a parameter. Thus, the large scale structure that is controlled by the inviscid terms can be completely described in terms of D^*. At the other end of the spectrum of length scales, it is obviously necessary to capture the largest geometrical features needed to define the enclosure fire scenario. Given current computing capability, the number of cells that can be incorporated in a given simulation is in the range of one to two million. Thus, the plume and enclosure scales must be roughly within an order of magnitude of each other. This implies that large fires can be studied using the present methodology in either small or large spaces, but small fires must be studied in proportionately small domains if the important features of the plume are to be captured. Given the rapid growth rate of computer power, these estimates can be expected to change substantially over the next four years.

With these ideas in mind, four examples illustrating the present capabilities of the approach outlined are presented. First, an isolated pool fire simulated with the use of thermal elements is shown in Fig. 1. The figure depicts a 25 cm

Fig. 1. A simulation of a buoyant diffusion flame, showing the three major zones of the fire: the continuous flame, intermittent and plume regions.
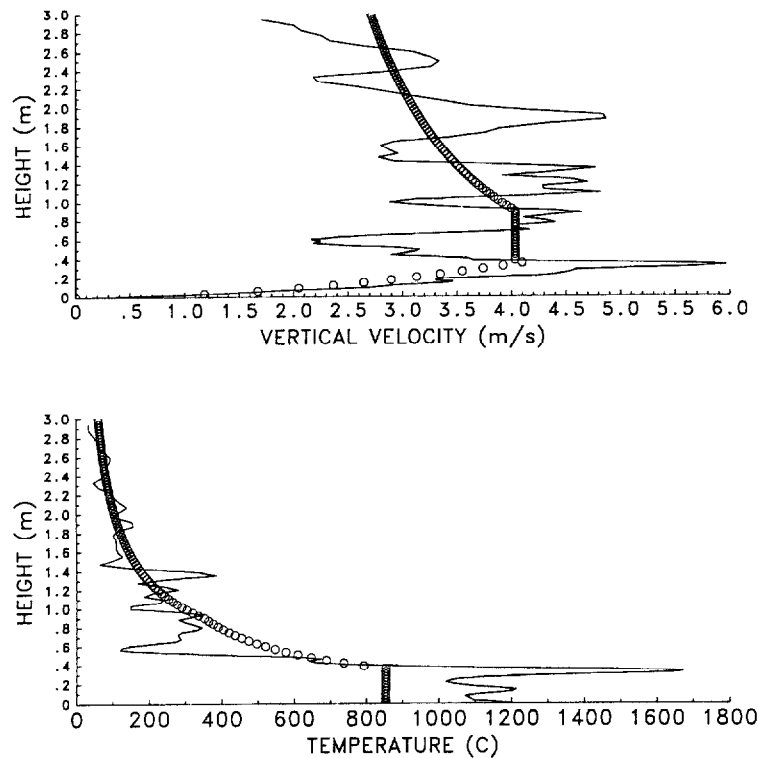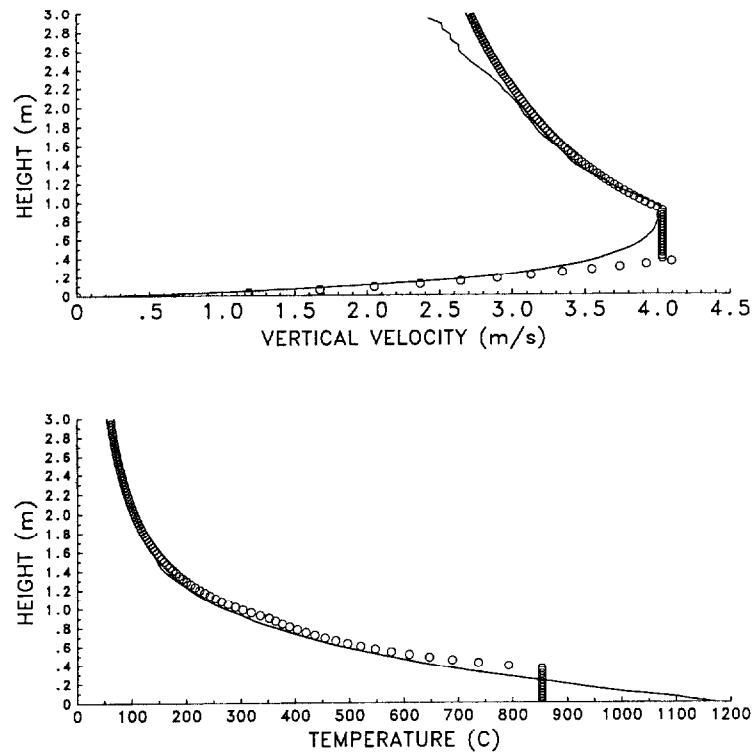
Fig. 2. A comparison of the instantaneous centerline velocity and temperature of a 45 kW pool
fire with the correlation of Baum and McCaffrey.

by 25 cm pool fire with a 45 kW heat release rate. The domain simulated is
1·5 m on a side and 3 m in height. A computational mesh of 96 × 96 × 96 cells
is employed with the grid cells gradually stretched in the vertical direction.
Three temperature contours are shown that correspond to the boundaries of
the continuous flame, intermittent flame, and plume zones as defined in Baum
and McCaffrey.[5] Figure 1 is an instantaneous snapshot of the fire, and
centerline profiles of the vertical velocity and temperature are shown in Fig. 2,
along with the correlation of Baum and McCaffrey. Of course, the correlation
represents time-averaged quantities, so a more appropriate comparison is
shown in Fig. 3, where now the results of the calculation are time-averaged as
well. The agreement is remarkably good, owing to the fact that the bulk of the
convective mixing has been captured directly. There are no empirical para-
meters in the calculation. Indeed, the fact that the *results* of the simulation can
be averaged in a routine way while the *equations* of fluid mechanics cannot is
the basis of the whole approach presented here.

Fig. 3. A comparison of the time-averaged centerline velocity and temperature of a 45 kW pool fire with the correlation of Baum and McCaffrey.

The next three calculations are of enclosure fire scenarios. First, a simulation of an enclosure fire experiment conducted by Steckler *et al.*[9,10] shows that reasonably good agreement with experimental results can be obtained at the levels of spatial resolution achievable with current CFD techniques and computer facilities. The overall geometry of the Steckler experiments is shown in Fig. 4. The grid used was made up of 160 × 96 × 72 cells roughly 3 cm on a side. The velocity vectors displayed in the vertical center plane after the flow has reached an apparent steady state are also shown. In addition to giving some idea of the overall flow pattern they give an indication of the spatial resolution achieved in the computation. The wireframe doorway velocity plot shows the characteristic orifice profile, with the maximum speed near the jet edge. This plot is remarkably similar to that given in Fig. 5 of Baum *et al.*,[4] where the experimental profiles are displayed. A quantitative comparison between theory and experiment is shown in Fig. 5, where time-averaged
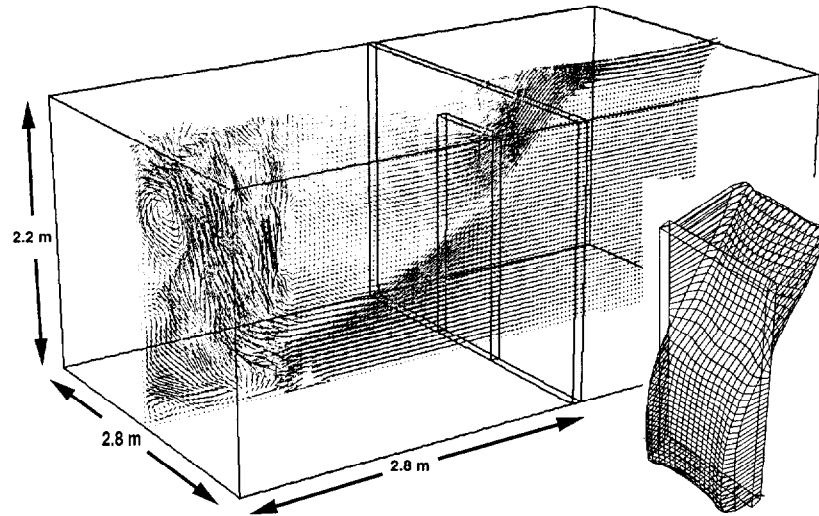
Fig. 4. Geometry of Steckler *et al.* experiment, showing the velocity vectors along a slice down the centerline of the configuration. Shown at the right is the velocity profile in the doorway.

doorway centerline velocity and temperature profiles are displayed. There are no adjustable parameters in the model, so the relatively good agreement between the measured and calculated results is an indicator of the *predictive* capability of the present approach.
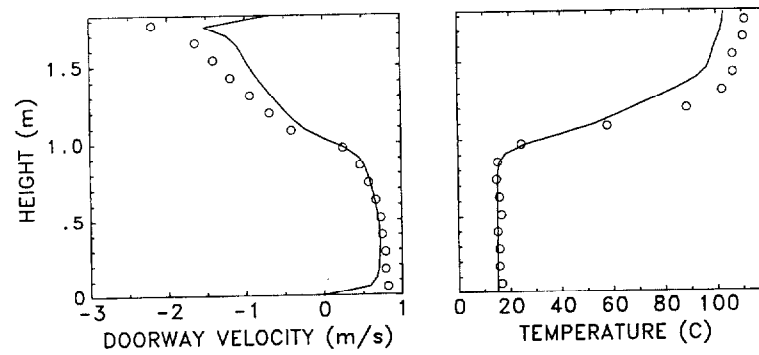

Fig. 5. Comparison of experimental (circles) and simulation (lines) centerline temperature and velocity profiles in the doorway of the Stecker experiment.

It has been argued that such fine resolution for a simple enclosure fire simulation is excessive. Indeed, the work of Kerrison *et al.*[11] shows that reasonably good agreement with Steckler's data can be obtained using the commercial CFD package FLOW3D on a grid of 8280 cells, distributed non-uniformly throughout the domain. The cost of these calculations is substantial, due in large part to the flexible nature of the grid structure and to the iterative nature of the algorithm. The algorithm described above, on the other hand, exploits the rectangular shape of most building geometries so that calculations on grids of over a million cells can be performed in comparable time to those performed by all-purpose codes using a few tens of thousands of cells. Given the nearly 100-fold increase in grid cells and using the blocking technique described above, it is possible to carve out regions of great geometrical complexity out of a rectangular solid and still maintain the efficiency of the algorithm. As a demonstration of this efficiency, a simulation of one of Steckler's experiments was performed using a uniform grid of 8640 cells. The transient calculation required about 20 CPU seconds per simulated second, with each simulated second requiring about 75 time steps. This calculation was performed on the IBM workstation described above, and platforms of comparable power are now available for a few tens of thousands of US dollars. There is also a more fundamental point to be considered. Even a perfectly resolved computation employing the $k-\epsilon$ or similar models will only produce a solution of the model equations. What relation such solutions have to time-averaged solutions of the Navier–Stokes equations is an open question. The approach described here, on the other hand, systematically captures more and more of the dynamic range contained in the Navier–Stokes equations as the spatial and temporal resolution is improved.

Next, experiments conducted in a much larger enclosure are simulated to demonstrate that smoke movement in large spaces can be described with reasonably high resolution. In November 1994, NIST conducted smoke transport experiments in the FRI test facility in Japan. The building was 20 m tall and 24 m on each side, with large vents near the floor and ceiling for controlling the ventilation. A number of 1·2 m and 2 m pan fires with different fuels were studied. One of the tests, a 2 m, 5 MW heptane fire, was simulated using a spatial grid of 96 × 96 × 72 cells to cover the entire facility. Figure 6 presents a view of the structure and the fire plume. Unfortunately, the dynamics of the fire plume cannot be conveyed by the picture, but the snapshot does show the bottleneck structure of the fire at one stage in the cycle. These pulsations manifest themselves in the centerline temperature traces. In the experiment, thermocouples were placed directly above the fire, and temperatures recorded every second. Figure 7 shows the experimental and simulated time histories of the temperature during the burn. The time traces
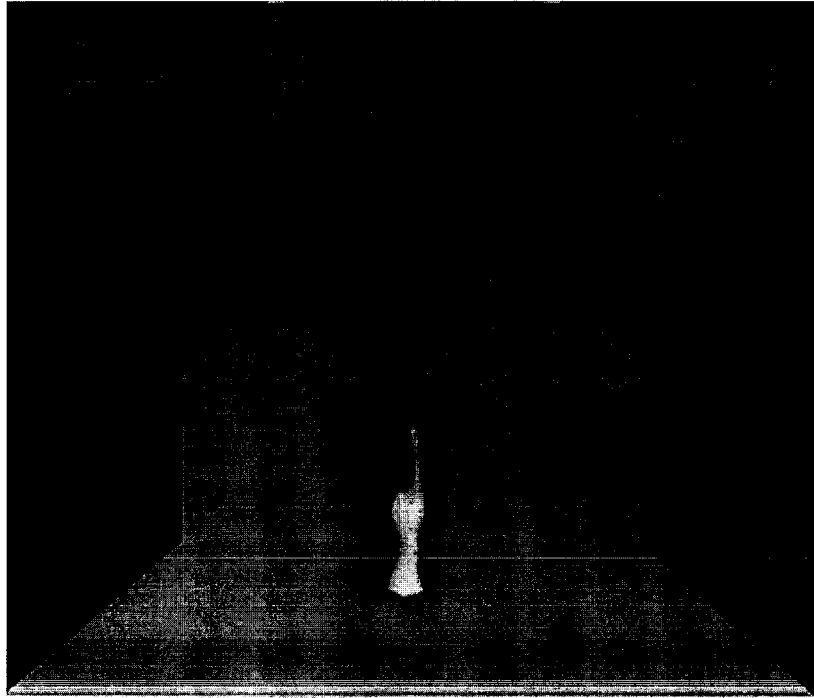
Fig. 6. Snapshot of a 5 MW heptane pool fire simulation of the FRI experiments. The building is 20 m high, and 24 m on each side. Three contours of temperature are shown, indicating roughly the location of the fire, the smoke plume and the ceiling layer.

have not been averaged so as to indicate the large fluctuations that are captured by the time-resolved calculations. Again, the explicit calculation of the large-scale fluctuations distinguishes this approach from others that use empirical models in averaged equations.

Finally, a study of smoke movement induced by a fire in a hypothetical hotel unit demonstrates the level of geometrical complexity that can be simulated at present. The smoke plume from a fire on top of a bed in an idealized hotel room unit is shown in Fig. 8. The unit also contains a sofa to the right of the bed, as well as a chest of drawers and a desk on the opposite wall. A closet blocked off from the rest of the unit and a bathroom with open doorway are to the left. Air heated 10°C above ambient enters the room at 25 cm/s through a duct on the lower right wall and is extracted on the upper left wall above a closed door with a gap at the floor. The vents operate at fixed outside pressures, so the inflow is reduced and outflow increased as the room
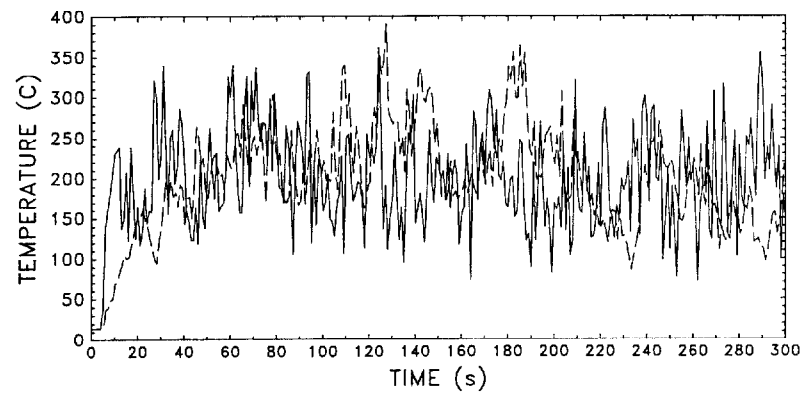
Fig. 7. Comparison of experimental (dotted line) and simulated temperature (solid line) time histories 9 m above a 5 MW heptane fire.

pressure rises due to the fire. The overall grid is composed of $192 \times 96 \times 64$ 4 cm^3 cubes. The calculation simulates about one min of real time. These computations required approximately 20 μs per cell per time step on an IBM RS 6000/58H server, and used 280 Mbytes of memory.
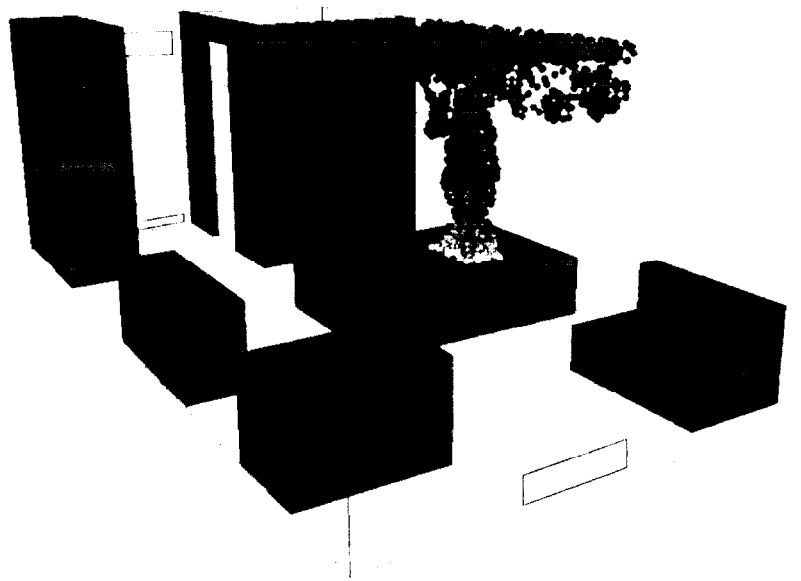

Fig. 8. Simulation of a hotel room fire, with ignition occurring on the bed. The dots represent thermal elements that originate at the bed.

6 CONCLUSIONS

The methodology and sample results presented in this paper are intended to demonstrate that smoke movement caused by enclosure fires of practical interest can be calculated with a rather high degree of accuracy with no empirical inputs. Present capabilities permit fully three-dimensional simulations on grids exceeding one million cells, permitting the resolution of length scales that are two orders of magnitude down from the length of the enclosure. Numerical simulations of small-scale and large-scale experiments have compared favorably with experimental data and correlations. Since there are no adjustable parameters in the model, the good agreement indicates the usefulness of the code as a *predictive* tool.

REFERENCES

1. Patankar, S. V., *Numerical Heat Transfer and Fluid Flow*. Hemisphere, Washington, USA, 1980.
2. Smagorinsky, J., General circulation experiments with primitive equations—I. The basic experiment. *Monthly Weather Rev.*, 91 (1963) 99–105.
3. Rehm, R. G. & Baum, H. R., The equations of motion for thermally driven, buoyant flows. *J. Res. NBS*, 83 (1978) 297–308.
4. Baum, H. R., Rehm, R. G. & Gore, J. P., Transient combustion in a turbulent eddy. In *23rd Int. Symp. on Combustion*, The Combustion Institute, Pittsburgh, 1990, pp. 715–22.
5. Baum, H. R. & McCaffrey, B. J., Fire induced flow field-theory and experiment. In *Fire Safety Science, Proc. 2nd Int. Symp.* Hemisphere, New York, 1989, pp. 129–48.
6. McGrattan, K. B., Rehm, R. G. & Baum, H. R., Fire driven flows in enclosures. *J. Computational Physics*, 110 (1994) 285–91.
7. Baum, H. R., Ezekoye, O. A., McGrattan, K. B. & Rehm, R. G., Mathematical modeling and computer simulation of fire phenomena. *Theoretical and Computational Fluid Dynamics*, 6 (1994) 125–39.
8. Peyret, R. & Taylor, T. D., *Computational Methods for Fluid Flow*. Springer, New York, 1983.
9. Steckler, K. D., Quintiere, J. Q. & Rinkinen, W. D., Flow induced by a fire in a compartment. In *19th Int. Symp. on Combustion*, The Combustion Institute, Pittsburgh, 1982, pp. 913–20.
10. Steckler, K. D., Baum, H. R. & Quintiere, J. Q., Fire induced flows through room openings – flow coefficients. In *20th Int. Symp. on Combustion*, The Combustion Institute, Pittsburgh, 1984, pp. 1591–600.
11. Kerrison, L., Galea, E. R., Hoffmann, N. & Patel, M. K., A comparison of a FLOW3D based fire field model with experimental room fire data. *Fire Safety J.*, 23 (1994) 387–411.